HHS Public Access

Author manuscript

J Med Genet. Author manuscript; available in PMC 2021 June 21.

Published in final edited form as:

J Med Genet. 2018 February ; 55(2): 122–130. doi:10.1136/jmedgenet-2017-104827.

Defect in phosphoinositide signalling through a homozygous variant in *PLCB3* causes a new form of spondylometaphyseal dysplasia with corneal dystrophy

Salma Ben-Salem[#1], **Sarah M Robbins**[#2], **Nara LM Sobreira**[2], **Angeline Lyon**[3], **Aisha M Al-Shamsi**[4], **Barira K Islam**[5], **Nadia A Akawi**[6], **Anne John**[1], **Pramathan Thachillath**[5], **Sania Al Hamed**[5], **David Valle**[2], **Bassam R Ali**[1], **Lihadh Al-Gazali**[5]

[1]Department of Pathology, College of Medicine and Heath Sciences, University Al-Ain, Al Ain, AbuDhabi, United Arab Emirates

[2]Human genetics and Molecular Biology, Institute of Genetic Medicine, Johns Hopkins University School of Medicine, Baltimore, Maryland, USA

[3]Chemistry and Biological Sciences, West Lafayette, USA

[4]Department of Paediatrics, Tawam Hospital, Al-Ain, United Arab Emirates

[5]Department of Paediatrics, College of Medicine and Heath Sciences, United Arab Emirates University, Al Ain, United Arab Emirates

[6]Division of Cardiovascular Medicine, John Radcliffe Hospital, University of Oxford, Oxford, Oxfordshire, UK

[#] These authors contributed equally to this work.

Abstract

Background—Bone dysplasias are a large group of disorders affecting the growth and structure of the skeletal system.

Methods—In the present study, we report the clinical and molecular delineation of a new form of syndromic autosomal recessive spondylometaphyseal dysplasia (SMD) in two Emirati first cousins. They displayed postnatal growth deficiency causing profound limb shortening with

Correspondence to Professor Lihadh Al-Gazali, Department of Pediatrics, College of Medicine and Health Sciences, United Arab Emirates University Al-Ain, United arab emirates; l.algazali@uaeu.ac.ae.

Contributors All authors made a significant contribution to data collection, data interpretation and critical assessment of this study. Specifically, SBS, SMR, NlMS, DV, BRA and AL contributed to study design and concept. LA initiated the study, recruited the family, and performed clinical evaluations of the patients. AMA helped in patients assessment and clinical tests. SBS and NLMS analyzed WES data and Sanger sequencing. SBS and SMR performed functional studies. AL and BKI have done the molecular modeling. NAA and AJ helped in Sanger sequencing. SAH helped in blood sample collection. PT isolated the genomic DNA from blood samples. LA, DV and Bra coordinated the study. all authors read and approved the final manuscript.

Competing interests none declared.

Patient consent Obtained.

Ethics approval Al-Ain District Human Research Ethics Committees (protocol number ERH-2015-324115-115).

Provenance and peer review Not commissioned; externally peer reviewed.

► Additional material is published online only. To view please visit the journal online (http://dx.doi.org/10.1136/jmedgenet-2017-104827).

proximal and distal segments involvement, narrow chest, radiological abnormalities involving the spine, pelvis and metaphyses, corneal clouding and intellectual disability. Whole genome homozygosity mapping localised the genetic cause to 11q12.1–q13.1, a region spanning 19.32 Mb with ~490 genes. Using whole exome sequencing, we identified four novel homozygous variants within the shared block of homozygosity. Pathogenic variants in genes involved in phospholipid metabolism, such as *PLCB4* and *PCYT1A,* are known to cause bone dysplasia with or without eye anomalies, which led us to select *PLCB3* as a strong candidate. this gene encodes phospholipase c β 3, an enzyme that converts phosphatidylinositol 4,5 bisphosphate (PIP_2) to inositol 1,4,5 triphosphate (IP_3) and diacylglycerol.

Results—The identified variant (c.2632G>T) substitutes a serine for a highly conserved alanine within the Ha2' element of the proximal C-terminal domain. This disrupts binding of the Ha2' element to the catalytic core and destabilises PLCB3. Here we show that this hypomorphic variant leads to elevated levels of PIP_2 in patient fibroblasts, causing disorganisation of the F-actin cytoskeleton.

Conclusions—Our results connect a homozygous loss of function variant in *PLCB3* with a new SMD associated with corneal dystrophy and developmental delay (SMDCD).

INTRODUCTION

Chondrodysplasias are a large group of conditions affecting the skeleton, often associated with other systemic abnormalities. Classification of chondrodysplasias is usually based on clinical, radiographic and molecular findings.[12] In the last decade, molecular studies have identified hundreds of genes responsible for the different forms of chondrodystrophies.[3] These disorders are relatively common among the United Arab Emirates (UAE) population with a rate of 9.46 skeletal dysplasias in 10 000 births.[4] Studies of families from UAE led to the identification of several rare and new forms of chondrodysplasia.[5–11] Spondylometaphyseal dysplasias (SMDs) are a rare form of chondrodysplasia characterised by severe abnormalities in vertebrae and metaphyses of tubular bones. Ophthalmological abnormalities have been reported in only two types of SMDs: SMD cone rod dystrophy (SMDCRD, MIM 608940)[1213] and axial SMD with retinal degeneration (MIM 602271).[14] Cone rod dystrophy is a feature of SMDCRD which is caused by loss-of-function variants in *PCYT1A*. This gene encodes CCTα, a vital component of the Kennedy phospholipid biosynthesis pathway.[1213] In axial SMD, the ophthalmological abnormalities include retinitis pigmentosa with optic atrophy which can lead to progressive visual impairment.[14] The molecular basis underlying axial SMD is currently unknown.

Here, we report a consanguineous family from UAE with a new autosomal recessive (AR) SMD associated with intellectual disability and corneal dystrophy (SMDCD) caused by a homozygous variant in *PLCB3*. This enzyme (EC 3.1.4.11) catalyses the production of diacylglycerol (DAG) and inositol 1,4,5 triphosphate (IP_3) from phosphatidylinositol 4,5 bisphosphate (PIP_2).[15] PLCB3 is activated by two G-protein α subunits (α-q and α−11), as well as G-protein β and γ subunits.[16] Phospholipase C (PLC) enzymes play crucial roles in inflammation, cell growth, signalling, cell death and maintenance of membrane phospholipids.[17] Abnormalities in PLCs and their downstream targets have been associated with a wide range of congenital human disorders, including skeletal disorders.[1218–21] In this

study, the identified *PLCB3*:NM_000932:c.2632G>T variant destabilises the protein and reduces its enzymatic activity, leading to PIP_2 accumulation. Patient fibroblasts are significantly larger with a weaker F-actin network and more punctuate appearance. This phenotype is strikingly similar to Lowe syndrome (MIM 309000) fibroblasts, which also display actin abnormalities due to defects in phosphoinositide signalling.[2223] Our findings establish *PLCB3* as the gene responsible for SMDCD and highlight the importance of phosphoinositide signalling in the development of the skeleton, brain and eye.

METHODS

Family ascertainment

We identified a consanguineous Emirati family with two affected cousins IV-1 and IV-3 (figure 1). We recruited the parents and other family members and obtained informed written consents from all participants in this study.

Genome mapping and molecular analysis

Blood samples were collected and gDNA was isolated using Flexigene DNA extraction kit (Qiagen Gmbh, Germany) according to the manufacturer's instructions. Comparative Genomic Hybridization (CGH) array analysis and data interpretation were carried out as a service by Sengenics (http://www.sengenics.com/). Sister chromatid exchange assay and karyotyping were performed as a service by Mayo Clinic (http://www.mayoclinic.org/) and Tawam Hospital's Cytogenetics Laboratory (Al-Ain), respectively.

Affymetrix SNP array V.6.0 was used to genotype all participants in this family according to the manufacturer's protocols (Affymetrix, Santa Clara, California, USA). The Affymetrix GCOS software has been used for quality control analysis and data formatting. SNP genotypes were determined using the GTYPE Affymetrix program using the default settings (Affymetrix, Santa Clara, California, USA). Linkage analyses were performed using Homozygosity Mapper (http://www.homozygositymapper.org/) under the assumption of an AR mode of inheritance and complete penetrance of disease allele.[24] Short tandems repeat (STR) markers were used to confirm and narrow down the potential region of homozygosity. All STR markers primers from HG19/GRCh37 are listed in ssupplementary table 1. PCR amplification conditions and genotyping protocols[25] are available upon request. Fragment analyses were evaluated on the ABI Prism 3130xl, and data were inspected using GeneMapper software V.4.1.1 (Applied Biosystems, USA). Sanger sequencing was performed according to standard protocols.

Exome capture, sequencing and variant prioritisation

Whole exome sequencing (WES) was performed in both affected children (IV-1 and IV-3) using Illumina HiSeq 2000 (Illumina, USA). WES was carried out by the Baylor-Hopkins Center for Mendelian Genomics (www.mendeliangenomics.org). Variant filtering was performed using the PhenoDB Variant Analysis tool.[26] We captured the CCDS exonic regions and flanking intronic regions totalling ~51 Mb by using the Agilent Sure-Select XT kit and generated paired end 100 bp reads with the Illumina HiSeq2500 platform. We aligned each read to the HG19/GRCh37 human genome reference with Burrows-Wheeler

Alignment V.0.5.10-tpx.[27] Local realignment and base call quality score recalibration were performed using the Genome Analysis Toolkit V.2.3–9-ge5ebf34.[28] Variant filtering was performed using the Variant Quality Score Recalibration method.[29] The average exome coverage was between 79 and 95 reads per base for each family member sequenced, with at least 90% of all targets covered at 30x in all family members. Ninety-nine per cent of all targets were covered at 8x in all family members. All variants were subject to variant prioritisation in our local UAE WES data, local Baylor-Hopkins Center for Mendelian genomics sequencing data, gnomAD (gnomad.broadinstitute.org), and the National Heart, Lung, and Blood Institute (NHLBI) Exome Variant Server (EVS) (http://evs.gs.washington.edu/EVS/). Prediction analyses of amino acid substitutions impact on the structure and function of proteins, were examined using PROVEAN, Stanford Information Filtering Tool (protein prediction tool) (SIFT), Polyphen2 (Hum Var), MutationTaster, ConSurf and Combined Annotation Dependent Depletion (Protein Prediction tool) (CADD) (table 1). Our initial filtering criteria for whole exome data were as follows: homozygous non-synonymous SNV not in dbSNP126, 129 or 131 with population frequency less than 1% in EVS and 1000 Genomes (http://www.internationalgenome.org/) with both copies shared only by the affected cousins, as well as highly conserved at the DNA and amino acid levels and predicted ‘damaging’ by the above in silico tools.

Molecular modelling

Crystallographic Object-Oriented Toolkit (*Coot*)[30] was used to generate the p.A878S variant in the structure of the $G\alpha_q$-PLCβ3-Δ882 complex (Protein Data Bank (PDB) ID: 3OHM), which was solved to 2.0 Å and is the highest resolution structure published to date.[31] The p.A878S variant was simulated, and the structure was analysed for steric clashes.

Cell culture and transient transfection

Primary adherent fibroblast cells were derived from skin biopsy from patient IV-1. The pCMV6-PLCB3 plasmid was obtained from Origene (#RC224268). Site directed mutagenesis was performed using the KOD Hot Start Master Mix (EMD Millipore, #71842–3). Transient transfection was performed in COS-7 cells, which has no endogenous expression of PLCB3, using Lipofectamine 2000 (ThermoFisher Scientific #11668027) according to the manufacturer’s instructions.

Western blot analysis

Cells were lysed using 0.5% NP-40 lysis buffer. Total protein was estimated using bicinchoninic acid assay (BCA) assay kit (Pierce cat #23225) according to the manufacturer’s instructions. 20 μg of protein was subjected to 4%–15% gradient sodium dodecyl (lauryl) sulfate-polyacrylamide gel electrophoresis (SDS-PAGE) and transferred electrophoretically to a polyvinylidene difluoride (PVDF) membrane. After blocking for 1 hour at room temperature (RT), the membrane was incubated with primary rabbit anti-PLCB3 antibody (Abcam #ab73998) overnight at 4°C. After washing with tris-buffered saline and tween 20 solution (TBST), the membrane was incubated for 1 hour with antirabbit IgG antibody conjugated with horseradish peroxidase (HRP) (Abcam #ab6721). Then, the blot was developed using Super Signal enhanced chemiluminescence (ECL) kit

(ThermoFisher Scientific, #34095) followed by exposure to X-ray film. Glyceraldehyde 3-phosphate dehydrogenase (GAPDH) was used as loading control.

Immunocytochemistry

Patient and control fibroblasts were grown on coverslips until approximately 40%–50% confluent. Wheat germ agglutinin (WGA) (ThermoFisher Scientific, #W32464), Alexa Fluor-488 conjugated phalloidin (ThemoFisher Scientific, #A12379), anti-PLCB3 antibody (Abcam #ab73998), anti-PtdIns(4,5)P2 antibody (Echelon Biosciences, #Z-P045) and Alexa Fluor-488 secondary antibody (ThermoFisher Scientific, #A-21042) were used following the manufacturer's protocol. For cytochalasin D (ThermoFisher Scientific, #PHZ1063) treatment, cells were treated with a final concentration of 1 μM, and then stained with phalloidin antibody. After staining using the primary antibody, cells were counterstained with 4',6-diamidino-2-phenylindole (DAPI) (ThermoFisher Scientific, #D1306) and mounted with Prolong Gold antifade mountant (ThermoFisher Scientific, #P36930). Blinded to genotype, images were taken using the Zeiss ZSM-700 confocal microscope. Images were scored for each cell matching the scoring criteria as described previously.[32] This method classifies F-actin staining into four patterns (types a, b, c and d) on the basis of the number and length of actin stress fibres: type (a) cells have longer, more densely packed actin stress fibres, type (b) have fine cables and at least two heavy distinct cables, type (c) have only fine stress fibres and type (d) have no detectable stress fibres in the central area of the cells.[32]

RESULTS

Clinical features of a new SMD with corneal dystrophy and intellectual disability

Patient IV-1 (figure 1A–i) was a 1185 gr (>25th centile) male product of a 22-year-old woman (III-2) whose 29 weeks pregnancy was normal until the onset of premature labour. Prenatal ultrasound revealed short limbs and narrow thorax. The baby was floppy at birth and required intubation and ventilation. His birth length was 32 cm (<3rd centile) and head circumference 27.5 cm (>50th centile). On examination, he had short limbs, with proximal and distal segments involved. The fingers and toes were short and the chest narrow (figure 1B). There was hypertelorism, prominent eyes, depressed nasal bridge and short upturned nose. He was noted to have bilateral corneal clouding on day 12. Skeletal survey (figure 1B) showed short long bones with wide metaphyses and some coarse trabecule at the metaphyses. There was cupping of the distal end of the radius and ulna (figure 1B). The distal epiphysis of the femur and proximal epiphysis of tibia were not calcified. There was shortening of all metacarpal and metatarsal bones. The talus and calcaneus had abnormal appearance with spurs. The ribs appeared short with a wide anterior aspect. The lumbar and thoracic vertebrae had beaks at their anterior aspects, and the intervertebral spaces were wide. The iliac bones were abnormal, almost square and short with medial projections (figure 1B). Echocardiography showed a large patent ductus arteriosus, which eventually required surgical correction. Basic screening for storage disease including white blood cell inclusions, urine mucopolysaccharides and oligosaccharides was negative. The baby had a stormy neonatal period and was difficult to wean off the ventilator due to the narrow chest and hypoplastic lungs. He eventually required tracheostomy. Brain and renal ultrasounds were normal. Opthalmological examination revealed bilateral corneal haziness with normal

retinas. The child had bilateral corneal grafting at the age of 6 months followed by tarsorrhaphy and keratoplasty. Repeat skeletal survey at the age of 2 years showed evidence of SMD (figure 1B). At the age of 4 years, the proband's weight was 14 kg (<3rd centile) and height was 85 cm (<<3rd centile). He is developmentally delayed and has chronic lung disease with chronic respiratory failure requiring a tracheostomy and continuous oxygen supplementation. He also has a gastrostomy tube to counteract chronic gastro-oesophageal reflux and repeated aspiration pneumonia. Currently, he is 6 years old with severe developmental delay. He can roll over and can sit without support but cannot sustain weight on his legs. He is totally wheelchair bound and dependent on his parents and caregiver. He has blurred vision due to the corneal opacities. He can hear and understand words, but displays no speech or meaningful babbling, only occasional moaning sounds. Recent routine clinical tests such as plasma proteins, lipid profile, plasma amino acids, blood phosphorus, alkaline phosphatase and parathyroid hormone, urinalysis and urine organic acids, were all normal.

Patient IV-3 was a 1190 gr (50th centile) male product of a 21-year-old woman (III-4) (figure 1A–ii). The pregnancy was complicated by placenta previa, leading to preterm delivery by lower section caesarean section at 27 weeks. Birth length was 35 cm (10th centile), and head circumference 25.5 cm (>10th centile). The infant was floppy at birth and required intubation and ventilation. He had short limbs with short fingers and toes and dysmorphic features, including hypertelorism, prominent eyes with corneal clouding, depressed nasal bridge and a short upturned nose. Ophthalmological evaluation showed bilateral vascularised corneal opacities with central thickened white cream-coloured tissue and thinner greyish periphery; the surface of the cornea was epithelised. B-scan ultrasonography showed normal retinas, normal size optic nerves, clear vitreous and normal posterior lens. The chest was narrow. Echocardiography revealed a large patent ductus arteriosus with left to right shunt. Brain CT scan showed a choroid plexus cyst on the right side. He had continuous stridor and bronchoscopy showed mild laryngomalacia. Skeletal survey showed abnormalities similar to that of his male cousin (patient IV-1) (figure 1B). He had corneal grafting of the right eye followed by the left eye, but he experienced graft rejection. He had chronic lung disease with pulmonary hypertension and was oxygen dependent. He died at the age of 8 months of septic shock.

Exclusion of large structural chromosomal abnormalities and localisation of the genetic cause to 11q12.2

In patient IV-1, karyotype and sister chromatid exchange test were normal. An array comparative genomic hybridization (aCGH) analysis showed structural variation gains at 10q26.3 (g.135242631–135377956[4]) and 14q23.3 (g.66257688–66978807[3]) based on genome build HG19/GRCh37. aCGH analysis in the parents showed that parents III-2 and III-4 carry the CNV gain on 10q26.3, while parents III-2 and III-3 have the CNV gain on 14q23.3. Based on these results, we considered these CNVs to be non-pathogenic. Given that the radiological features, particularly the shape of ilium, were similar to Schneckenbecken dysplasia (OMIM 269250), we sequenced *SLC35D1* but did not find any pathogenic variants in the coding or splice site regions of this gene in our patients.

Subsequently, we performed whole genome homozygosity mapping in participants (III-1, III-2, III-3, III-4, IV-2, IV-4 and IV-5) and patients (IV-1 and IV-3) and identified a large homozygous region on chromosome 11 shared only by the affected children (figure 2A). This region spans approximately 19.3 Mb divided into two intervals flanked by SNPs rs835764-rs8186206 and rs4939000-rs4247634. This interval encompasses 487 known genes, 89 located in the first interval and 398 in the second (figure 2A). Genotyping using STR markers D11S1313, D11S4076, D11S1883 and D11S1889 confirmed the linkage of SMDCD to 11q12.1–q13.1 (figure 2B). All four parents (III-1, III-2, III-3 and III-4) and all healthy children (IV-2, IV-4 and IV-5) were heterozygous for all tested STR markers, most captured SNPs and sequenced variants within this region (figure 2B).

WES revealed a pathogenic homozygous *PLCB3* variant within the linked interval

WES in both affected children (IV-1 and IV-3) identified a total of six novel rare variants: *CELF1 (*NM_198700:c.833A>G:p. N278S), *PRPF19* (NM_014502.4:c.807C>G:p.S269R*), FEN1 (*NM_004111.5:c.475G>A:p.A159T*), INCENP (*NM_001040694.1:c.1469G>A:p.R490Q*), PLCB3* (NM_000932.2:c.2632G>T:p.A878S) and *CETN2* (NM_004344:c.G473A:p.S158N). These were the only variants identified that were homozygous in both affected cousins and heterozygous in all obligate carrier parents, and healthy siblings. All variants and their segregation in the family were confirmed using Sanger sequencing. First, we excluded the involvement of variants in *CELF1* (MIM# 160900) and *CETN2* (MIM# 300006) genes because (1)the clinical features associated with these genes did not overlap with our patient phenotype, (2) sister chromatid exchange assay was normal, and (3)they did not lie within the linked interval. Four variants in *PRPF19, FEN1, INCENP* and *PLCB3* were located within the linkage region on 11q12.1–q13.1 (figure 2B). Only the patients (IV-1 and IV-3) were found to be homozygous for these variants, while all healthy individuals were heterozygous (figure 2B). To determine which variant was responsible for SMDCD in this family, we examined each variant as follows. The *PRPF19* gene encodes the human homolog of yeast *Pso4*, a gene essential for cell survival and DNA repair.[33] The c.807C>G variant was not found in 100 matched control samples, nor in ExAC (http://exac.broadinstitute.org/). The flap endonuclease, *FEN1*, is an evolutionary conserved gene for DNA replication. The c.475G>A variant is not listed in EVS, nor in dbSNP, but was reported once as heterozygous (with minor allele frequency (MAF)=1.511e-05) in ExAC. *Fen1* deficiency causes instability of the genome and trinucleotide repeat expansion.[34] We excluded the involvement of *FEN1* on the basis of the normal sister chromatid exchange assay in patient IV-1. *INCENP* encodes a regulatory protein in the chromosome passenger complex. The c.1469G>A variant was not detected in 200 healthy chromosomes from the same ethnic group and not listed in dbSNP, but was reported once as heterozygous in ExAC. INCENP plays a pivotal role in the regulation of cell division.[35] Staining using H&E on patient fibroblast cells was normal with no increase of multinucleated cells. In addition, expression of exogenous flag-tagged-INCENP-WT/ p.R490Q in HeLa cells showed normal subcellular localisation when compared with control (see online Supplementary file 2). Moreover, cell proliferation assay of patient cells using Brdu cell proliferation kit (Abcam) was normal (see online Supplementary file 3). Based on these experiments we considered the variants in *FEN1*, *INCENP* and *PRPF19* unlikely to be the cause of our patients' phenotype.

The *PLCB3* c.2632G>T variant was not present in 200 healthy chromosomes from the same ethnic background, and it was not listed in dbSNP databases nor in EVS. However, the variant has been reported in the heterozygous state with an MAF of 1.824e-05 in ExAC. Together with a second heterozygous variant (c.2632G>A:p.A878T), the total multiallelic variance at c.2632 has a frequency of 6.385e-05<0.01 in ExAC. The MAF cut-off for AR conditions is less than 1% since causal variants are rare in such condition.[36] The Variant Effect Predictor (http://asia.ensembl.org/Tools/VEP) calculates the evolutionary conservation of c.2632G>T. This variant affects all three different coding isoforms of *PLCB3,* and this position is highly conserved at the DNA and protein levels between vertebrates and mammalians (figure 2D). Plcb3, originally isolated from rat brain, is widely expressed, with the highest concentrations found in brain, the pituitary gland, liver and parotid gland.[37] Additionally, zebra fish embryos showed high expression of Plcb3 in bone and cartilage, as well as in neural crest cells, kidney cells and neurons.[38] *Plcb3* null mutants in zebra fish showed abnormal skeletal patterning with malformed facial and thoracic bones. [39] In mice, targeted disruption of *plcb3* results in embryonic lethality.[40] However, further *Plcb3* knockout models showed discordant results.[3641] These discrepancies might be explained by the manner in which the *plcb3* gene was disrupted.[3641] We conclude that c.2632G>T is extremely rare, conserved, and is likely pathogenic according to the American College of Medical Genetics and Genomics (ACMG) variant classification guidelines.[42]

Loss of PLCB3 activity causes PIP_2 accumulation and F-actin destabilisation mimicking a Lowe syndrome phenotype

To evaluate the functional consequences of the *PLCB3* variant, we first performed molecular modelling based on the crystal structure of the $G\alpha_q$-PLCβ3-Δ882 complex (PDB ID: 3OHM). The para and trans rotomers of the introduced serine side chain are predicted to result in steric clashes with residues in the catalytic core, specifically p.T758 and p.R760 (figure 2E). These structural abnormalities may result in reduced catalytic activity and impaired ability of Hα2'[1] to efficiently bind to the catalytic core under basal conditions. The p.A878S variant may also lead to local structural rearrangements within this region, as serines are known to destabilise α helices (figure 2E).[43] In addition, the importance of this position is clear, as variants in residues adjacent to p.A878, such p.L879A, decrease the global stability of PLCB3.[43]

To confirm these predictions, we performed Western blotting on cell lysate from COS-7 cells transiently transfected with either PLCB3-WT or PLCB3-A878S. These blots showed 95% reduction in PLCB3-p.A878S protein levels as compared with PLCB3-WT (n=3, figure 3A), confirming that PLCB3-p.A878S is a hypomorphic variant that appears to decrease PLCB3 levels in the cell (figure 3A,B). Loss of PLCB3 activity (see online Supplementary file 4) would be expected to result in an accumulation of its substrate, PIP_2. Immunofluorescence assays against PIP_2 in patient fibroblasts showed a marked increase in PIP_2 levels compared with passage-matched control fibroblasts (figure 3C). Patient fibroblasts also showed increased nuclear localisation of PIP_2 (figure 3C–h), whereas no nuclear aggregation was observed in control fibroblasts (figure 3C–c).

Interestingly, Lowe syndrome (MIM 309000) also exhibits PIP_2 accumulation, but by an alternate mechanism affecting PIP_2 5-phosphatase, which catalyses PIP_2 breakdown.[44] Lowe patient fibroblasts show dysregulation of the actin cytoskeleton, including a higher proportion of cells with a weak F-actin network, an increase in punctate F-actin staining and an enhanced sensitivity to actin depolymerising agents.[22] In view of this, we hypothesised that loss of *PLCB3* activity would lead to similar morphological alterations in patient fibroblasts. Immunostaining of lectin fibres showed that patient fibroblasts (figure 3B–f) are significantly larger when compared with controls (figure 3B–a) ($p<0.05$, t-test) (figure 3B). Next, we evaluated the F-actin network in these cells using green fluorescent protein (GFP)-phalloidin, which binds to F-actin. Quantification of the F-actin staining in patient IV-1 fibroblasts showed a significant overall decrease in actin network strength compared with normal fibroblasts, which displayed mainly strong actin networks with thick cables (figure 3D–II, n=156 patients, 91 controls, $\chi^2=12.909$, df=3, $p<0.001$). Patient fibroblasts also showed more punctuate staining (as vizualised on figure 3D–IP), highlighting very short fibres, when compared with controls (figure 3D-III, n=156 patients, 91 controls, $\chi^2=23.27$, df=3, $p<0.001$). Next, we treated patient cells using cytochalasin D, which prevents the addition of new actin monomers and causes overall filament shortening. Patient fibroblasts (figure 3B–j) showed increased sensitivity to stress compared with controls (figure 3B–e) under the same stress (figure 3B). Overall, this work suggests that loss of *PLCB3* function is responsible for PIP_2 accumulation and dysregulation of the actin cytoskeleton in patient fibroblasts (figure 3).

DISCUSSION

Phospholipases are large group of enzymes that hydrolyse phospholipids into fatty acids and other lipophilic substances. These enzymes play crucial roles in various cellular process including hormone secretion, neurotransmitter signal transduction, cell growth, membrane trafficking, ion channel activity, regulation of the cytoskeleton, cell cycle control and apoptosis.[17] The PLC enzyme) family consists of six subfamilies, with a total of 13 different isoenzymes differentially expressed throughout the human body.[37] This specificity suggests a precise role for each PLC subtype in its particular tissue. PLCs have been associated so far with various human disorders that affect the brain, skeleton, heart and immune system.[1945–47] In this study, we report for the first time the implication of a PLC in a new bone disorder, termed SMDCD, in Emirati patients.

Here, we identified a homozygous missense variant (c.2632G>T) in *PLCB3*, resulting in the substitution of p.A878S in the proximal C-terminal domain. The change occurs within the autoinhibtory Ha2' helix element (figure 2C), a region crucial for the activation and stabilisation of PLCB3 (figure 4). Variants affecting residues involved in the Gαq ligand binding and/or residues interacting with the catalytic domain have been shown to destabilise PLCB3 and disrupt its autoinhibition.[43] We showed that the p.A878S variant results in a hypomorphic allele which reduces the total level of PLCB3, leading to a loss of enzymatic activity (figure 3, Supplementary file 4). Immunocytochemical quantification of PIP_2 levels in patient's fibroblasts showed a striking increase of PIP_2 when compared with controls (figure 3C–d,i). In this experiment, we also observed punctate accumulations of PIP_2 in the nucleus; the significance of this aggregation is unclear (figure 3C–f). PIP_2 is known to

control many cell processes such as cell signalling, protein trafficking and particularly cytoskeleton remodelling.[48] On activation by cell surface receptors, PLCB3 cleaves PIP_2 to yield the signal molecules IP_3 and DAG (figure 4). Specifically, IP_3 mediates activation of Ca^{2+} and calmodulin, which in turn activates actin severing proteins such as cofilin and gelosin, resulting in disorganisation of the F-actin cytoskeletal network (figure 4).[49] PIP_2 is also involved in the regulation of several actin regulatory proteins.[50] PIP_2 accumulation affects the morphology of our patient fibroblasts, which show thinner microfilaments and shorter bundles with more punctuate appearance, suggestive of short F-actin bundles and less packed microfilaments (figure 3D). Moreover, these fibroblasts displayed an enhanced sensitivity to cytochalasin D compared with controls, also suggesting shorter actin filaments (figure 3B–e–j).

Lowe syndrome is characterised by bilateral cataracts, intellectual disability and renal Fanconi syndrome. Our patients show some shared clinical abnormalities with patients with Lowe syndromesuch as short stature, intellectual disability and cloudy cornea. Though most patients with Lowe syndrome display bilateral cataracts, there are a few cases with other ocular abnormalities, including corneal opacity.[51] Kidney dysfunction of the Fanconi type, which is seen in Lowe syndrome, is usually slow and progressive.[51] At present, patient IV-1 does not display any renal dysfunction, but we cannot rule out the onset of this condition in the future.

To the best of our knowledge, this is the first study to implicate PLCB3 in a new form of SMDCD in humans. The p.A878S variant disrupts a vital regulatory region of PLCB3. Moreover, we show that decreased PLCB3 protein levels alter the F-actin network due to PIP_2 accumulation in affected fibroblasts. Therefore, we suggest a common pathway involved in phospholipid metabolism, Ca^{2+} homoeostasis and cytoskeleton organisation that controls bone, brain and eye development. Further studies may elucidate the particular molecular mechanism of phospholipid dysregulation in the pathogenicity of such disorders.

Supplementary Material

Refer to Web version on PubMed Central for supplementary material.

Acknowledgements

The authors thank the patients and their family members for their participation in this research study. The authors also thank Mr Saeed Tariq for his contribution to electron microscopy analyses.

Funding the laboratories of LA and BRA are funded by the United Arab Emirates University (grant #31M241). This work was also supported by NHGRI grants 2T32GM07814 to the Baylor-Hopkins center for Mendelain genomics and UM1HG006542.

ASHG 2016 by SMR as poster presentation: PgmNr 2339, Oct 18-22, Vancouver, CANADA.

REFERENCES

1. Superti-Furga A, Unger S. Nosology and classification of genetic skeletal disorders: 2006 revision. Am J Med Genet A 2007;143a:1–18. [PubMed: 17120245]
2. Warman ML, Cormier-Daire V, Hall C, Krakow D, Lachman R, LeMerrer M, Mortier G, Mundlos S, Nishimura G, Rimoin DL, Robertson S, Savarirayan R, Sillence D, Spranger J, Unger S, Zabel B,

Superti-Furga A. Nosology and classification of genetic skeletal disorders: 2010 revision. Am J Med Genet A 2011;155a:943–68. [PubMed: 21438135]

3. Gilissen C, Hoischen A, Brunner HG, Veltman JA. Disease gene identification strategies for exome sequencing. Eur J Hum Genet 2012;20:490–7. [PubMed: 22258526]
4. Al-Gazali LI, Bakir M, Hamid Z, Varady E, Varghes M, Haas D, Bener A, Padmanabhan R, Abdulrrazzaq YM, Dawadu A, Abdulrrazzzaq YM, Dawodu AK. Birth prevalence and pattern of osteochondrodysplasias in an inbred high risk population. Birth Defects Res A Clin Mol Teratol 2003;67:125–32. [PubMed: 12769508]
5. al Gazali LI, Devadas K, Hall CM. A new lethal neonatal short limb dwarfism. Clin Dysmorphol 1996;5:160–4.
6. al-Gazali LI, Aziz SA, Salem F. A syndrome of short stature, mental retardation, facial dysmorphism, short webbed neck, skin changes and congenital heart disease. Clin Dysmorphol 1996;5:321–7. [PubMed: 8905197]
7. al-Gazali LI, Dawodu AH, Hamada M, Bakir M, Bakalinová D. Severe facial clefting, limbic dermoid, hypoplasia of the corpus callosum, and multiple skin appendages: severe frontofacionasal “dysplasia” or newly recognised syndrome? Am J Med Genet 1996;63:346–7. [PubMed: 8725783]
8. Akawi NA, Al-Gazali L, Ali BR. Clinical and molecular analysis of UAE fibrochondrogenesis patients expands the phenotype and reveals two COL11A1 homozygous null mutations. Clin Genet 2012;82:147–56. [PubMed: 21668896]
9. Akawi NA, Ali BR, Al-Gazali L. Stüve-Wiedemann syndrome and related bent bone dysplasias. Clin Genet 2012;82:12–21. [PubMed: 22300393]
10. Bayoumi R, Saar K, Lee YA, Nürnberg G, Reis A, Nur-E-Kamal M, Al-Gazali LI. Localisation of a gene for an autosomal recessive syndrome of macrocephaly, multiple epiphyseal dysplasia, and distinctive facies to chromosome 15q26. J Med Genet 2001;38:369–73. [PubMed: 11389160]
11. Al-Kindi A, Kizhakkedath P, Xu H, John A, Sayegh AA, Ganesh A, Al-Awadi M, Al-Anbouri L, Al-Gazali L, Leitinger B, Ali BR. A novel mutation in DDR2 causing spondylo-meta-epiphyseal dysplasia with short limbs and abnormal calcifications (SMED-SL) results in defective intra-cellular trafficking. BMC Med Genet 2014;15:42. [PubMed: 24725993]
12. Hoover-Fong J, Sobreira N, Jurgens J, Modaff P, Blout C, Moser A, Kim OH, Cho TJ, Cho SY, Kim SJ, Jin DK, Kitoh H, Park WY, Ling H, Hetrick KN, Doheny KF, Valle D, Pauli RM. Mutations in PCYT1A, encoding a key regulator of phosphatidylcholine metabolism, cause spondylometaphyseal dysplasia with cone-rod dystrophy. Am J Hum Genet 2014;94:105–12. [PubMed: 24387990]
13. Yamamoto GL, Baratela WA, Almeida TF, Lazar M, Afonso CL, Oyamada MK, Suzuki L, Oliveira LA, Ramos ES, Kim CA, Passos-Bueno Mr, Bertola Dr. Mutations in PCYT1A cause spondylometaphyseal dysplasia with cone-rod dystrophy. Am J Hum Genet 2014;94:113–9. [PubMed: 24387991]
14. Isidor B, Baron S, Khau van Kien P, Bertrand AM, David A, Le Merrer M. axial spondylometaphyseal dysplasia: confirmation and further delineation of a new SMD with retinal dystrophy. Am J Med Genet A 2010;152a:1550–4. [PubMed: 20503334]
15. Berridge MJ, Irvine RF. Inositol trisphosphate, a novel second messenger in cellular signal transduction. Nature 1984;312:315–21. [PubMed: 6095092]
16. Rebres RA, Roach TI, Fraser ID, Philip F, Moon C, Lin KM, Liu J, Santat L, Cheadle L, Ross EM, Simon MI, Seaman We. Synergistic ca2+ responses by g{alpha} i- and g{alpha}q-coupled g-protein-coupled receptors require a single PLC{beta} isoform that is sensitive to both g{beta} {gamma} and g{alpha}q. J Biol Chem 2011;286:942–51. [PubMed: 21036901]
17. Cooper MG, Sunderland M. The cell: a molecular approach. 2nd ed, 2000.
18. Boyer O, Benoit G, Gribouval O, Nevo F, Pawtowski A, Bilge I, Bircan Z, Deschênes G, Guay-Woodford LM, Hall M, Macher Ma, Soulami K, Stefanidis CJ, Weiss R, Loirat C, Gubler MC, Antignac C. Mutational analysis of the PLCE1 gene in steroid resistant nephrotic syndrome. J Med Genet 2010;47:445–52. [PubMed: 20591883]
19. Kurian MA, Meyer E, Vassallo G, Morgan NV, Prakash N, Pasha S, Hai NA, Shuib S, Rahman F, Wassmer E, Cross JH, O’Callaghan FJ, Osborne JP, Scheffer IE, Gissen P, Maher ER.

Phospholipase C beta 1 deficiency is associated with early-onset epileptic encephalopathy. Brain 2010;133:2964–70. [PubMed: 20833646]

20. Rieder MJ, Green GE, Park SS, Stamper BD, Gordon CT, Johnson JM, Cunniff CM, Smith JD, Emery SB, Lyonnet S, Amiel J, Holder M, Heggie AA, Bamshad MJ, Nickerson DA, Cox TC, Hing AV, Horst Ja, cunningham ML. A human homeotic transformation resulting from mutations in PLCB4 and GNAI3 causes auriculocondylar syndrome. Am J Hum Genet 2012;90:907–14. [PubMed: 22560091]
21. Yu P, Constien R, Dear N, Katan M, Hanke P, Bunney TD, Kunder S, Quintanilla-Martinez L, Huffstadt U, Schröder A, Jones NP, Peters T, Fuchs H, De Angelis MH, Nehls M, Grosse J, Wabnitz P, Meyer TP, Yasuda K, Schiemann M, Schneider-Fresenius C, Jagla W, Russ A, Popp A, Josephs M, Marquardt A, Laufs J, Schmittwolf C, Wagner H, Pfeffer K, Mudde GC. Autoimmunity and inflammation due to a gain-of-function mutation in phospholipase C gamma 2 that specifically increases external ca2+ entry. Immunity 2005;22:451–65. [PubMed: 15845450]
22. Suchy SF, Nussbaum RL. The Deficiency of PIP2 5-Phosphatase in Lowe Syndrome Affects Actin Polymerization. Am J Hum Genet 2002;71:1420–7. [PubMed: 12428211]
23. Wymann MP, Schneiter R. Lipid signalling in disease. Nat Rev Mol Cell Biol 2008;9:162–76. [PubMed: 18216772]
24. Seelow D, Schuelke M, Hildebrandt F, Nürnberg P. HomozygosityMapper-an interactive approach to homozygosity mapping. Nucleic Acids Res 2009;37:W593–9. [PubMed: 19465395]
25. Schuelke M. An economic method for the fluorescent labeling of PCR fragments. Nat Biotechnol 2000;18:233–4. [PubMed: 10657137]
26. Sobreira N, Schiettecatte F, Boehm C, Valle D, Hamosh A. New tools for Mendelian disease gene identification: PhenoDB variant analysis module; and GeneMatcher, a web-based tool for linking investigators with an interest in the same gene. Hum Mutat 2015;36:425–31. [PubMed: 25684268]
27. Li H, Durbin R. Fast and accurate short read alignment with Burrows-Wheeler transform. Bioinformatics 2009;25:1754–60. [PubMed: 19451168]
28. McKenna A, Hanna M, Banks E, Sivachenko A, Cibulskis K, Kernytsky A, Garimella K, Altshuler D, Gabriel S, Daly M, DePristo Ma. The genome analysis Toolkit: a MapReduce framework for analyzing next-generation DNA sequencing data. Genome Res 2010;20:1297–303. [PubMed: 20644199]
29. DePristo MA, Banks E, Poplin R, Garimella KV, Maguire JR, Hartl C, Philippakis AA, Del Angel G, Rivas MA, Hanna M, McKenna A, Fennell TJ, Kernytsky AM, Sivachenko AY, Cibulskis K, Gabriel SB, Altshuler D, Daly MJ. a framework for variation discovery and genotyping using next-generation DNA sequencing data. Nat Genet 2011;43:491–8. [PubMed: 21478889]
30. Emsley P, Lohkamp B, Scott WG, Cowtan K. Features and development of Coot. Acta Crystallogr D Biol Crystallogr 2010;66(Pt 4):486–501. [PubMed: 20383002]
31. Waldo GL, Ricks TK, Hicks SN, Cheever ML, Kawano T, Tsuboi K, Wang X, Montell C, Kozasa T, Sondek J, Harden TK. Kinetic scaffolding mediated by a phospholipase C-beta and Gq signaling complex. Science 2010;330:974–80. [PubMed: 20966218]
32. Verderame M, Alcorta D, Egnor M, Smith K, Pollack R. Cytoskeletal F-actin patterns quantitated with fluorescein isothiocyanate-phalloidin in normal and transformed cells. Proc Natl Acad Sci U S A 1980;77:6624–8. [PubMed: 6256751]
33. Beck BD, Park SJ, Lee YJ, Roman Y, Hromas RA, Lee SH. Human Pso4 is a metnase (SETMAR)-binding partner that regulates metnase function in DNA repair. J Biol Chem 2008;283:9023–30. [PubMed: 18263876]
34. Zheng L, Dai H, Hegde ML, Zhou M, Guo Z, Wu X, Wu J, Su L, Zhong X, Mitra S, Huang Q, Kernstine KH, Pfeifer GP, Shen B. Fen1 mutations that specifically disrupt its interaction with PCNA cause aneuploidy-associated cancer. Cell Res 2011;21:1052–67. [PubMed: 21383776]
35. Cutts SM, Fowler KJ, Kile BT, Hii LL, O'Dowd RA, Hudson DF, Saffery R, Kalitsis P, Earle E, Choo KH. Defective chromosome segregation, microtubule bundling and nuclear bridging in inner centromere protein gene (incenp)-disrupted mice. Hum Mol Genet 1999;8:1145–55. [PubMed: 10369859]

36. Wang S, Zhou Y, Lukinius A, Oberg K, Skogseid B, Gobl A. Molecular cloning and characterization of a cDNA encoding mouse phospholipase c-beta3. Biochim Biophys Acta 1998;1393:173–8. [PubMed: 9714794]
37. Rebecchi MJ, Pentyala SN. Structure, function, and control of phosphoinositide-specific phospholipase C. Physiol Rev 2000;80:1291–335. [PubMed: 11015615]
38. Thisse B, Heyer V, Lux A, Alunni V, Degrave A, Seiliez I, Kirchner J, Parkhill JP, Thisse Spatial and temporal expression of the zebrafish genome by large-scale in situ hybridization screening. Methods Cell Biol 2004;77:505–19. [PubMed: 15602929]
39. Schilling TF, Piotrowski T, Grandel H, Brand M, Heisenberg CP, Jiang YJ, Beuchle D, Hammerschmidt M, Kane DA, Mullins MC, van Eeden FJ, Kelsh RN, Furutani-Seiki M, Granato M, Haffter P, Odenthal J, Warga RM, Trowe T, Nüsslein-Volhard C. Jaw and branchial arch mutants in zebrafish I: branchial arches. Development 1996;123:329–44. [PubMed: 9007253]
40. Wang S, Gebre-Medhin S, Betsholtz C, Stålberg P, Zhou Y, Larsson C, Weber G, Feinstein R, Oberg K, Gobl A, Skogseid B. Targeted disruption of the mouse phospholipase C beta3 gene results in early embryonic lethality. FEBS Lett 1998;441:261–5. [PubMed: 9883896]
41. Xie W, Samoriski GM, Mclaughlin JP, Romoser VA, Smrcka A, Hinkle PM, Bidlack JM, Gross RA, Jiang H, Wu D. Genetic alteration of phospholipase C beta3 expression modulates behavioral and cellular responses to mu opioids. Proc Natl Acad Sci USA 1999;96:10385–90. [PubMed: 10468617]
42. Amendola LM, Jarvik GP, Leo Mc, Mclaughlin HM, Akkari Y, Amaral MD, Berg JS, Biswas S, Bowling KM, Conlin LK, Cooper GM, Dorschner MO, Dulik MC, Ghazani AA, Ghosh R, Green RC, Hart R, Horton C, Johnston JJ, Lebo MS, Milosavljevic A, Ou J, Pak CM, Patel RY, Punj S, Richards CS, Salama J, Strande Nt, Yang Y, Plon SE, Biesecker LG, Rehm HL. Performance of ACMG-AMP Variant-Interpretation Guidelines among Nine Laboratories in the Clinical Sequencing Exploratory Research Consortium. Am J Hum Genet 2016;98:1067–76. [PubMed: 27181684]
43. Lyon AM, Tesmer VM, Dhamsania VD, Thal DM, Gutierrez J, Chowdhury S, Suddala KC, Northup JK, Tesmer JJ. An autoinhibitory helix in the C-terminal region of phospholipase c-β mediates Gαq activation. Nat Struct Mol Biol 2011;18:999–1005. [PubMed: 21822282]
44. Suchy SF, Nussbaum RL. The deficiency of PIP2 5-phosphatase in Lowe syndrome affects actin polymerization. Am J Hum Genet 2002;71:1420–7. [PubMed: 12428211]
45. Kido Y, Gordon CT, Sakazume S, Ben Bdira E, Dattani M, Wilson LC, Lyonnet S, Murakami N, Cunningham ML, Amiel J, Nagai T. Further characterization of atypical features in auriculocondylar syndrome caused by recessive PLCB4 mutations. Am J Med Genet A 2013;161a:2339–46. [PubMed: 23913798]
46. Zhou Q, Lee GS, Brady J, Datta S, Katan M, Sheikh A, Martins MS, Bunney TD, Santich BH, Moir S, Kuhns DB, ;Long Priel DA, Ombrello A, Stone D, Ombrello MJ, Khan J, Milner JD, Kastner DL, Aksentijevich I. A hypermorphic missense mutation in PLCG2, encoding phospholipase cγ2, causes a dominantly inherited autoinflammatory disease with immunodeficiency. Am J Hum Genet 2012;91:713–20. [PubMed: 23000145]
47. Oliveira TG, Di Paolo G. Phospholipase D in brain function and Alzheimer's disease. Biochim Biophys Acta 2010;1801:799–805. [PubMed: 20399893]
48. Insall RH, Weiner OD, Pip WOD. PIP3, PIP2, and cell movement--similar messages, different meanings? Dev Cell 2001;1:743–7. [PubMed: 11740936]
49. Logan MR, Mandato CA. Regulation of the actin cytoskeleton by PIP2 in cytokinesis. Biol Cell 2006;98:377–88. [PubMed: 16704377]
50. Hilpelä P, Vartiainen MK, Lappalainen P. Regulation of the actin cytoskeleton by PI(4,5) P2 and PI(3,4,5)P3. Curr Top Microbiol Immunol 2004;282:117–63. [PubMed: 14594216]
51. Gropman A, Levin S, Yao L, Lin T, Suchy S, Sabnis S, Hadley D, Nussbaum R. Unusual renal features of Lowe syndrome in a mildly affected boy. Am J Med Genet 2000;95:461–6. [PubMed: 11146467]

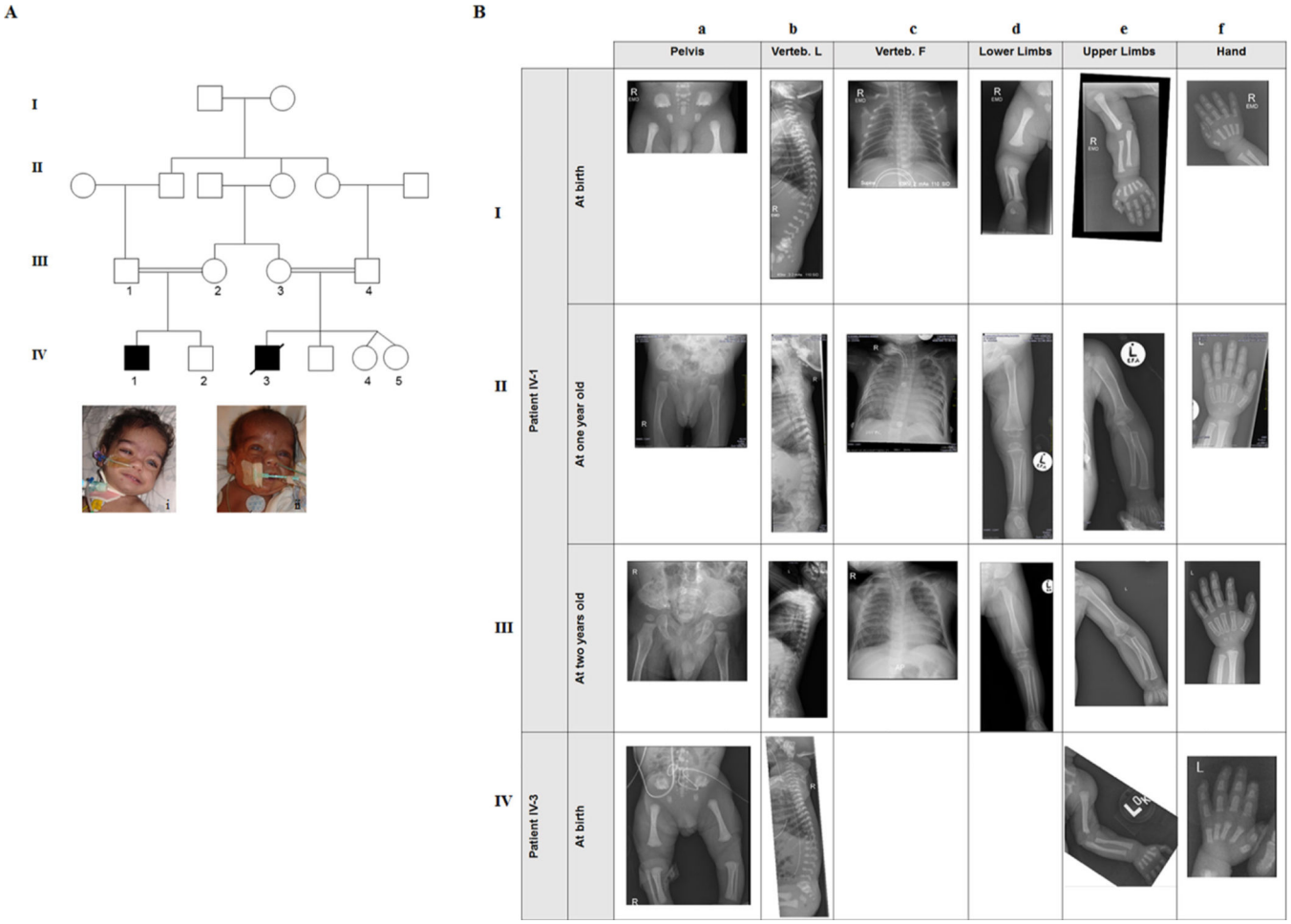

Figure 1.

Pedigree of a consanguineous Emirati family with two affected children. (A) Pedigree showing two first cousins with a new form of spondylometaphyseal dysplasia, intelectual disability (ID) and corneal dystrophy (SMDCD). i, photo of index patient IV-1; ii, photo of his cousin IV-3. (B) Skeletal survey summary of patients with the *PLCB3* variant. B-a, Pelvis: Patients (IV-1 and IV-3) since birth display abnormal iliac bones of pelvis which are square and short with medial projection (snail-like appearance). At 2 years of age, the iliac wings are short and irregular with lace-like appearance. There is coxa valga. B-b and B-c, Lateral and posterioranterior (AP) view of vertebrae: flat with abnormal shape of all lumbar and thoracic vertebrae with very wide intervertebral spaces and short and tiny ribs. B-d, Long bones of lower limbs: shortening of femur, tibia and fibula with widening and coarsetrabeculation of metaphyses, and generalized osteoporosis were noticed since birth. Note radiodense lines at the distal femur and tibia. B-e, Long bones of upper limbs: short long bones with wide metaphyses and coarse trabeculation. B-f, Hands: shortening of all metacarpal bones of the hands associated with osteoporosis.

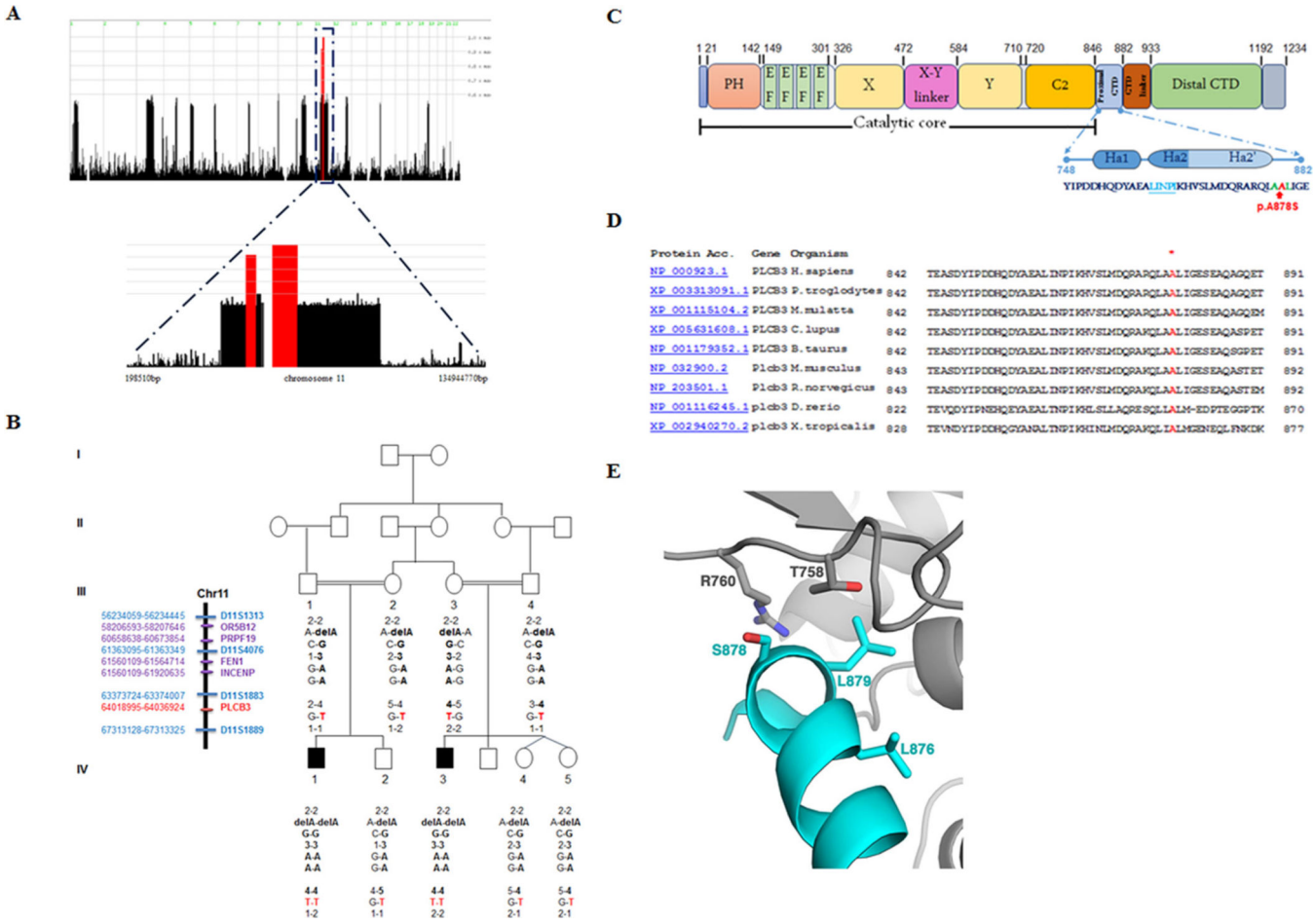

Figure 2.

Molecular analysis and computational analysis of the p.A878S variant. (A) Results of whole genome SNP mapping showing a single shared block of homozygosity (11p12.1-q13.1) in the affected children. (B) The homozygous region of 11.081MB limited by the STR markers D11S1313 and D11S1889 with segregation of all novel variants identified in *PRPF19, FEN1, INCENP and PLCB3* genes. Note that all variants were homozygous only in the affected children. (C) Schematic representation of different PLCB3 domains. A zoomed region from the proximal C-terminal domain (CTD) showing the p.A878S variant highlighted in red and marked by an arrow; surrounded by mutated residues at positions 877 and 879 indicated in green. the primary Gαq binding site in the proximal CTD is shown in blue. (D) Sequence alignments of different residues within the Ha2' helix region indicating that residue A878, shown in red, is highly conserved in different species. (E) Molecular model of the p.A878S variant in human PLCβ3. p.A878S was mutated in the Gαq-PLCβ3 structure (PDB ID 3OHM). The side chain of S878 is shown in the meta rotomer conformation, the only conformation in which the serine side chain does not sterically clash with the catalytic core, nor with residues R760 and T758. the Hα2' helix is shown in cyan and the PLCβ3 catalytic core is shown in grey.

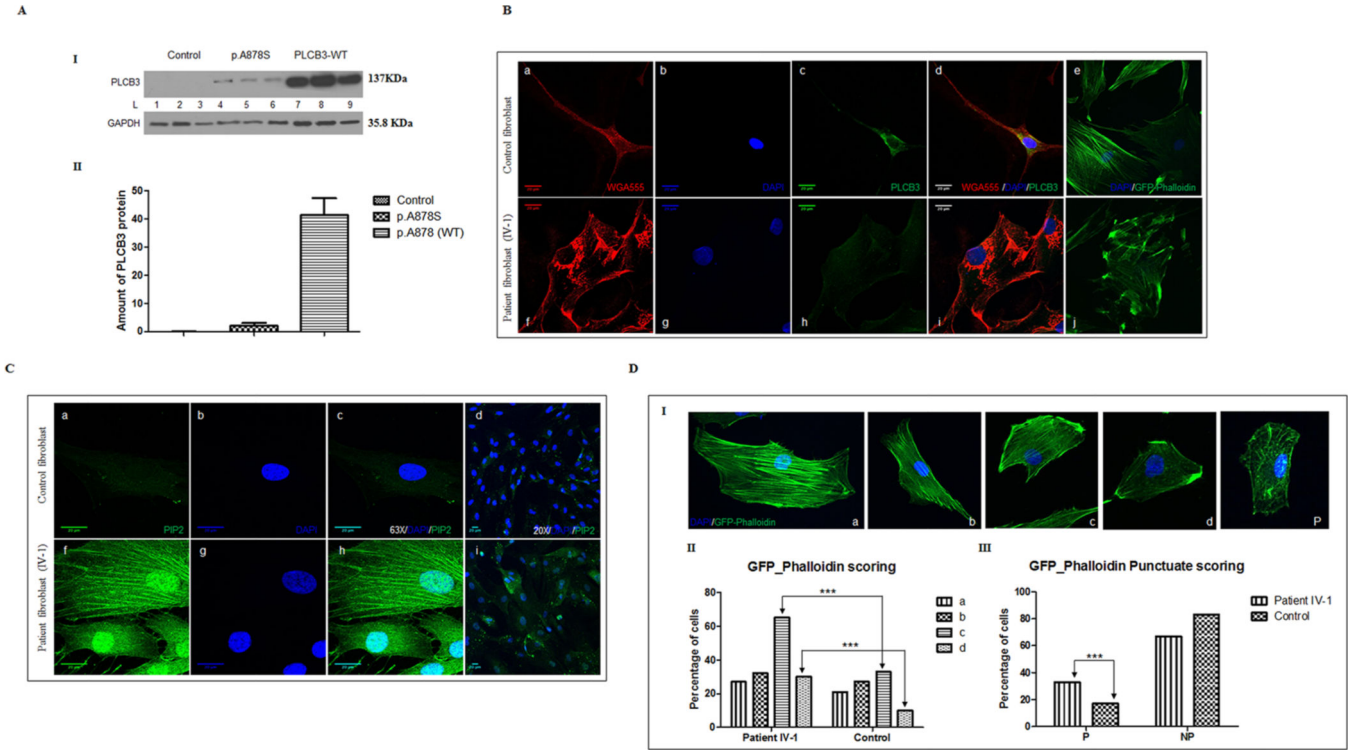

Figure 3.

Loss of PLCB3 activity causes accumulation of phosphatidylinositol 4,5 bisphosphate (PIP_2) and disorganisation of the actin cytoskeleton network. (A) Quantification of PLCB3 proteins levels in control, and patient fibroblasts as well as transiently transfected COS-7 cells. (A-I). Western blot showing the absence of endogenous expression of PLCB3 in COS-7 cells (lanes 1–3). Lanes 4–9 illustrate exogenous expression of *PLCB3* constructs. Mutant p.A878S proteins (lanes 4–6) showed weak expression of PLCB3 when compared with control (lanes 7–9). (A-II) PLCB3 protein levels estimated from the western blot results, t-test with n=3 independent trials. (B) Morphological abnormalities in patient fibroblasts due to PLCB3 deficiency. Lectin fibres are stained using fluorescently conjugated WGA555, and PLCB3 using anti-PLCB3 antibody (Abcam). Note the large size of patient fibroblasts (d–e) when compared with control (i–j) and the weak expression of PLCB3 in patient cells (h). Patient fibroblast (j) showing marked sensitivity to cytochalasin D treatment when compared with control (e). (c) Patient fibroblasts showing stringent increase in PIP_2 levels (f,h) compared with passage-matched control fibroblasts (a,c). Nuclei are counterstained with DAPI. (D) F-actin cytoskeleton network visualised using fluorescently labelled phalloidin (D–I). Immunohistochemistry images showing different F-actin staining patterns, type (a) cells have longer, more densely packed actin stress fibres (image D-Ia), type (b) have fine cables and at least two heavy distinct cables (image D-Ib), type (c) have only fine stress fibres (image D-Ic) and type (d) have no detectable stress fibres (image D-Id).[32] (D-II) Phalloidin scoring quantified using χ^2 test, n=156 patient fibroblasts, 91 control fibroblasts. Error bars are 1 SD. (D-III) Punctuate F-actin staining, as depicted on image (D-IP), was quantified using χ^2 test, n=156 patient fibroblasts, 91 control fibroblasts.

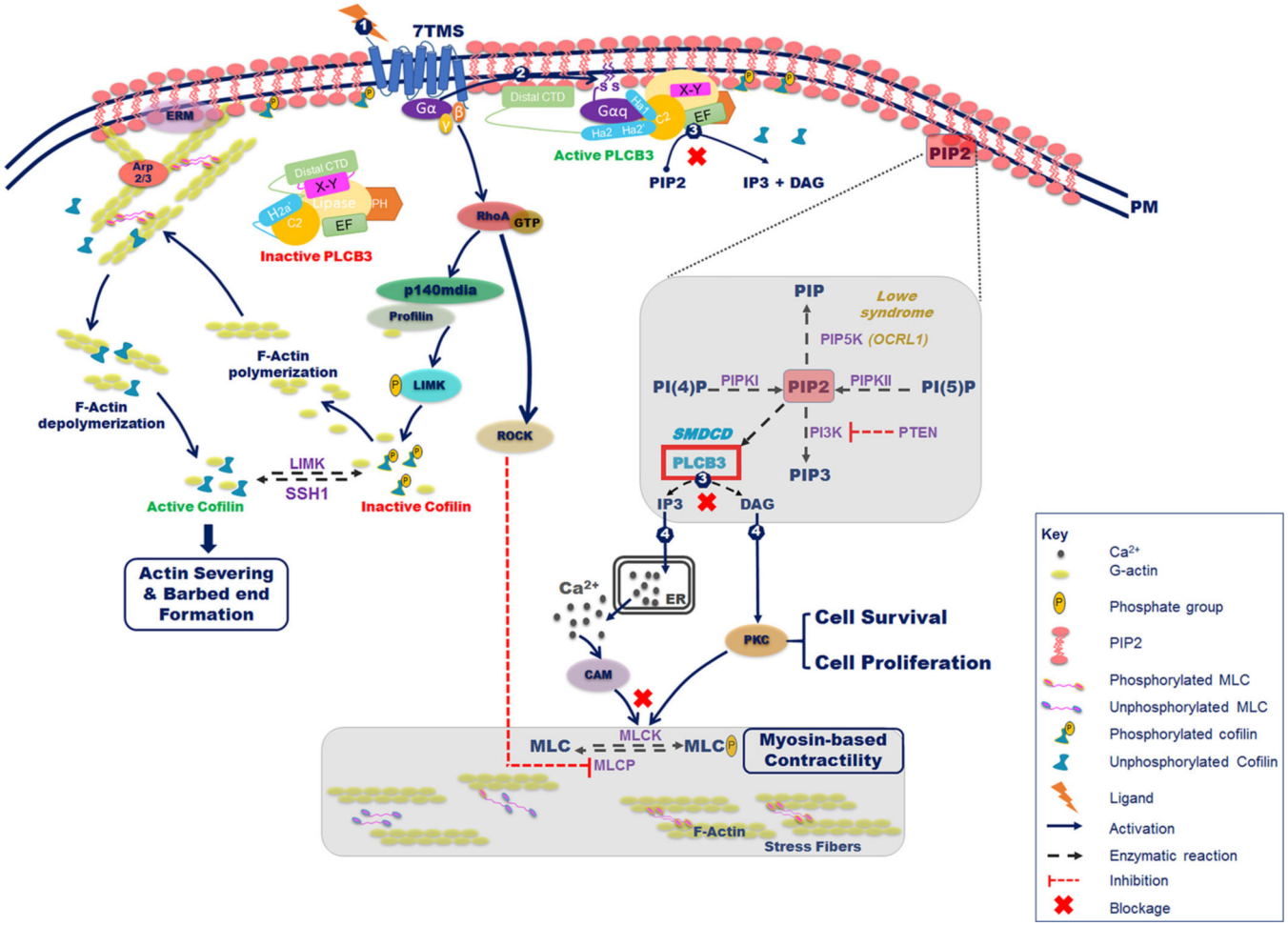

Figure 4.

Conformational change of PLCB3 on activation and phosphatidylinositol 4,5 bisphosphate (PIP_2) involvement in cytoskeleton organisation. Inactive PLCB3 in the left is in an autoinhibited state. Ha2' and the X-Y linker are bound to the catalytic core, while the distal C-terminal domain (CTD) domain is interacting with the cell membrane (once the enzyme is in the membrane) or the hydrophobic ridge of the catalytic core (once the enzyme in cytosol). Upon ligands binding, PLCB3 is activated by Gαq(*1*), leading to PLCB3 conformational changes (*2*) through displacement of Ha2' and recruitment of catalytic core to cell membrane. This activation converts membrane lipid Ptdins(4,5)P_2 (PIP_2) to second messengers diacylglycerol (DAG) and inositol 1,4,5 triphosphate (IP_3) (*3*). IP3 releases and increases the cytosolic concentration of calcium (Ca^{2+}) in the endoplasmic reticulum (ER). Ca^{2+} release regulates the binding of myosin to actin filaments, and activates the phosphorylation of the myosin light chain (MLC). Both IP_3 and DAG activate protein kinase C (PKC) which in turn controls cell proliferation and survival (*4*). Cofilin phosphorylation is driven by LIM-domain kinase (LIMK) and its dephosphorylation is mediated by the slinghshot 1 (SSH1). in our study, the p.A878S variant causes loss of PLCB3 activity leading to PIP_2 accumulation and resulting in disorganisation of the F-actin cytoskeletal network. PIP5K, PIP_2 5-phosphatase; PI3K, phosphoinositide 3-kinase; PIP3,

PtdIns(3,4,5)P3; PI(4)P, phosphatidylinositol 4-phosphate; PI(5)P, phosphatidylinositol 5-phosphate; PIPKI and PIPKII, phosphatidylinositol phosphate kinases I and II, respectively; PTEN, phosphatase and tensin homolog.

Table 1

In silico prediction analyses of the six identified variants by WES

Gene name	*SIFT*	*PolyPhen2*	*CADD (PHRED)*
CELF1	0.42	0	0.323
PRPF19	0.22	0.022	18.06
FEN1	0	1	28.4
INCENP	0.01	0.954	26.3
PLCB3	0.06	0.023	18.49
CETN2	1	0	5.746

SIFT, 0 is deleterious, 1 is tolerated. PolyPhen2: 0 is benign, 0.15 is possibly damaging, 1 is damaging. CADD: 0 is benign, 10 is top 10% of deleterious substitutions, 20 is top 1%.

PHRED, Phil's Read Editor.